GA–A26918

THE GENERAL ATOMICS FUSION THEORY

FINAL REPORT TO THE U.S. DEPARTMENT OF ENERGY

FOR THE PERIOD JANUARY 15, 2008 THROUGH JANUARY 14, 2011

by
PROJECT STAFF

OCTOBER 2010

GENERAL ATOMICS

DISCLAIMER

GA–A26918

THE GENERAL ATOMICS FUSION THEORY

FINAL REPORT TO THE U.S. DEPARTMENT OF ENERGY

FOR THE PERIOD JANUARY 15, 2008 THROUGH JANUARY 14, 2011

by
PROJECT STAFF

Work supported by
the U.S. Department of Energy
under DE-FG02-95ER54309

GENERAL ATOMICS PROJECT 03726
OCTOBER 2010

ABSTRACT

The objective of the fusion theory program at General Atomics (GA) is to significantly advance our scientific understanding of the physics of fusion plasmas and to support the DIII–D and other tokamak experiments as well as ITER research activities. The program plan is aimed at contributing significantly to the Fusion Energy Science, the Tokamak Concept Improvement, and ITER goals of the Office of Fusion Energy Sciences (OFES). Significant progress was made in each of the important areas of our research program during the last grant period GY08-10. This includes Development of the EPED1 predictive models for the H-mode pedestal height and width and validation against discharges from DIII-D, JET, C-Mod and other tokamaks, development of a unified framework to study tokamak plasma response including resistive and rotational effects below the Alfven frequency based on an extended energy principle, demonstration that the runaway-electron loss fraction reduces with an increase in the device size with a set of NIMROD 3D MHD simulations of mitigated disruptions in DIII-D, C-Mod, and ITER, validation of the new trapped gyro-Landau fluid (TGLF) transport model with comprehensive physics including general magnetic geometry and finite beta, development of a kinetic transport framework, TGYRO, which can run GYRO or TGLF together with the neoclassical code NEO for experimental validation studies as well as predictive simulation, demonstration using GYRO that zonal-flow induced pressure-profile corrugations can cause the instability rate of kinetic ballooning modes to sharply increase at half the ideal MHD critical β and is the long sought cause of the subcritical β limit, demonstration with a partial core-pedestal optimization using EPED1.6 and TGLF that suggests ITER should be able to achieve high performance operation, and development of an integrated modeling and fitting tool IMFIT to support tokamak research and operation.

TABLE OF CONTENTS

1. HIGHLIGHTS OF THEORY WORK IN GY08–10

During the past 3 years, significant progress was made in each of the important areas of our research program:

- Development of the EPED1 predictive models for the H-mode pedestal height and width based on stability of the peeling-ballooning mode, kinetic ballooning mode, and a diamagnetic model and validation against discharges from DIII-D, JET, JT-60U, and C-Mod.
- Detailed peeling-ballooning and local ballooning analysis of a DIII-D ITER demonstration discharge showing that the pedestal climbs slowly towards the peeling-ballooning instability boundary, and that ELM triggering corresponds to crossing the peeling-ballooning threshold.
- Demonstration with a partial core-pedestal optimization using the EPED1.6 pedestal model and TGLF core predictions that suggests ITER should be able to achieve high performance operation.
- Validation of the new trapped gyro-Landau fluid (TGLF) transport model with comprehensive physics including general magnetic geometry and finite beta with significantly improved experimental agreement over its predecessor GLF23.
- Development of a new TGLF collision model that demonstrates much better agreement against a large database of collisional GYRO simulations and successfully tested against a database of DIII-D and JET hybrid discharges.
- Demonstration with TGLF modeling studies of DIII-D ITER demonstration discharges that there is a noticeable reduction in the electron energy transport across the entire radius due to finite β and little change in the ion channel.
- Application of the new APS09 version of TGLF to examine the impact of the new collision model on the ITER baseline scenario fusion performance and the results obtained are close to those previously found using the GLF23 transport model.
- Development of a kinetic transport framework, TGYRO, which can run GYRO or TGLF together with the neoclassical code NEO for both experimental transport and flow validation studies, as well as predictive simulation.
- Demonstration using GYRO that zonal-flow induced pressure-profile corrugations can cause the instability rate of kinetic ballooning modes to sharply increase at half the ideal MHD critical β and is the long sought cause of the subcritical β limit.
- Demonstration with GYRO simulations that a mechanism based on symmetry breaking from profile variation (shear in temperature and density gradients) accounts for a

significant part of the residual stress momentum flow in a DIII-D discharge with no toroidal rotation.

- Development of a new eigenvalue solver for GYRO that drastically reduces the matrix size and storage requirement and provides an efficient tool for studying compressional magnetic perturbations.
- Addition of compressional magnetic perturbations to GYRO and associated discovery of high-k Alfven drift-wave cascades.
- Discovery that electromagnetic turbulence causes destruction of magnetic surfaces leading to stochastic electron transport broadly in agreement with GYRO-computed electromagnetic flux.
- Observation of global ITG modes across the *n*-spectrum in GYRO initial-value simulations in a variety of experimental plasmas using Miller model equilibria.
- Identification of energetic particle modes (EPMs) and toroidal Alfvén eigenmodes (TAEs) in a beam-heated, shear-reversed DIII-D discharge at low values of toroidal mode number *n* using GYRO.
- Demonstration with GYRO simulations that the onset of energetic-particle transport from long-wavelength TAE/EPM turbulence embedded in shorter-wavelength ITG/TEM turbulence does not degrade the background plasma confinement.
- Sonic capability added to the NEO neoclassical code.
- Demonstration with NEO studies of deuterium flow in the edge of DIII-D L-mode plasmas that indicate the flow remains essentially neoclassically driven even close to the edge and the carbon velocities do not fully reflect the deuterium velocities in the edge.
- Demonstration in a new analytical calculation that the poloidal electric field contribution can increase the neoclassical toroidal angular momentum flux by the order of the square root of the aspect ratio.
- Analytic calculation of second-order neoclassical distribution function in both the banana and Pfirsch-Schluter regimes including nonlinear collision operator.
- Development of a new tool VGEN to compute the radial electric field based on NEO for input to GYRO, TGYRO, and subsequent NEO calculations.
- Development of a unified framework to study tokamak plasma response including resistive and rotational effects below the Alfven frequency based on an extended energy principle that minimizes free energy of the plasma together with the external coils.

- Demonstration using the extended energy principle that tokamak response to external magnetic perturbations without resonances can be well approximated by the vacuum response and at resonances small resistivity and rotation can lead to near ideal response with screening and suppression of normal field.
- Demonstration that the runaway-electron loss fraction reduces with an increase in the device size with a set of 3D NIMROD simulations of mitigated disruptions in DIII-D, C-Mod, and ITER including drift-motion calculation for a test population of runaway electrons.
- Demonstration using the 3D MHD code NIMROD that in DIII-D discharges runaway electron (RE) loss mechanism differs for limited versus diverted shape and that the bulk $n = 1$ motion to the center column in the limited case results in a $n = 1$ RE striking pattern consistent with the experiments.
- Implementation of resistive wall boundary conditions into the 3D MHD code M3D-C1 and demonstration of initial benchmark calculations of kink modes that show good agreement with expected growth rates.
- Successful calculations of linear plasma response to applied non-axisymmetric fields for a series of DIII-D experiments using M3D-C1 including two-fluid effects.
- Demonstration that an applied negative surface voltage together with modest density increase is effective to erode the runaway electron current in ITER using an analytical model for runaway electron after a massive particle injection.
- Demonstration that coupled Monte-Carlo RF orbit and full-wave simulations with finite-orbit width and iterations between ion distribution and ICRF wave field are crucial to reproduce the enhanced neutron reaction, spectra, and outward spatial shifts of fast-ion distribution in DIII-D and NSTX HHFW experiments.
- Demonstration using kinetically reconstructed EFIT equilibria from DIII-D counter ECCD discharges that the tearing stability index Δ' and the saturated 3/2 island width increase strongly with a narrow ECCD width around the $q = 3/2$ surface consistent with experimental observations.
- Development of an analytical description of tokamak single and double null divertor equilibrium using the homogeneous solution of the Grad-Shafranov equation together with a particular Solovev-like solution.
- Demonstration with an EFIT study that fine spatial-grid equilibria generally satisfy the force balance constraint better and that the equilibrium iteration algorithm is related to the flux-control spatial feedback stabilization of the plasma.

- Development of an integrated modeling and fitting tool IMFIT to support tokamak research and operation and management of modeling tasks that is based on PYTHON and the Task Flow Architecture with extensive Graphical User Interfaces.
- Release of a first IMFIT public version with extensive GUI support to manage equilibrium, transport, and stability codes.
- Development of a method to compute steady-state solutions suitable for computationally intensive turbulent confinement models such as TGLF using an efficient hybrid approach and incorporation into ONETWO.

As a consequence of these results, scientists from the Theory Group were selected to give a number of invited talks and colloquia as highlighted in the next section. Sections 3–6 provide more detailed descriptions of the advances and achievements made in each of the major areas. A list of publications is given in Section 7.

2. SIGNIFICANT PRESENTATIONS IN GY08–10

2010 PRESENTATIONS

52nd APS DPP meeting in Chicago, IL November 8–12, 2010:

- G.M. Staebler gives an invited presentation "Discoveries from the Exploration of Gyro-kinetic Momentum Transport."

23rd IAEA Fusion Energy Conference in Daejon, Korea October 11–16, 2010:

- E.M. Bass gives a presentation "Gyro-kinetic Simulations of Energetic Particle Driven TAE/EPM Transport Embedded in ITG/TEM Microturbulence."
- M. Choi gives a presentation "Finite Orbit Monte-Carlo Simulation of ICRF Heating Scenarios in DIII-D, NSTX, KSTAR, and ITER."
- M.S. Chu gives a presentation "Response of a Resistive and Rotating Tokamak to External Magnetic Perturbations below the Alfven Frequency."
- V.A. Izzo gives an oral presentation "Runaway Electron Confinement Modeling for DIII-D, Alcator C-Mod, and ITER."
- J.E. Kinsey gives an oral presentation "ITER Predictions Using the GYRO Verified and Experimentally Validated TGLF Transport Model."
- P.B. Snyder gives an oral presentation "A First Principles Predictive Model of the Pedestal Height and Width: Development, Testing, and ITER Optimization with the EPED Model."

International Sherwood Fusion Theory Conference in Seattle, WA April 19–21, 2010:

- N. Ferraro gave an oral presentation "Extended MHD Calculations of Ideal and Non-Ideal ELM Stability."
- V.A. Izzo gave an oral presentation "Runaway Electron Confinement Modeling for DIII-D Disruptions."
- R.E. Waltz gave an oral presentation "Nonlinear Subcritical MHD Beta Limit."

FSP Workshop in Boulder, CO March 15, 2010:

- J. Candy gave a presentation "Transport-Timescale Plasma Core Simulations."
- P.B. Snyder gave a presentation "The Pedestal Science Driver."

US Transport Task Force Workshop in Annapolis, MD April 13–16 2010:

- E.M. Bass gave an oral presentation "Soft Threshold TAE/EPM Energetic Particle Transport Simulated in GYRO."
- P.B. Snyder gave an oral presentation "Update on EPED Model of the Pedestal Height and Width and Comparison to Experiment."

5th US-PRC Magnetic Fusion Collaboration Workshop in Wuhan, China May 5–7, 2010:

- L.L. Lao gave a presentation "Status and Progress in the Development of the IMFIT Integrated Modeling Tool to Support Tokamak Research and Operation."
- G. Li gave a presentation "Testing of Resistive MHD Models against Counter-ECCD Driven Tearing Modes in DIII-D."
- Q. Ren gave a presentation "High Spatial-Resolution Equilibrium Reconstruction and its Force Balance Analysis."

37th European Physical Society Conference on Plasma Physics in Dublin, Ireland, June 21–25, 2010:

- A.D. Turnbull gave a presentation "Giant Sawteeth in DIII-D and the Quasi-Interchange Mode."

2nd Integrated Modeling Expert Group Annual Meeting in ITER Headquarters Cadarache, France September 6–8, 2010:

- L.L. Lao gave a presentation "Status: IMFIT Integrated Modeling and Fitting Project."

C-Mod/NSTX Workshop in Princeton, NJ September 7, 2010:

- P.B. Snyder gave a presentation "The EPED Pedestal Model and Proposed Tests on Alcator C-Mod and NSTX."

RF SciDAC Workshop at PPPL in Princeton, NJ September 14–16, 2010:

- M. Choi gave a presentation "Status/Plans for Coupled Monte-Carlo and ICRF Full-Wave Solvers."

2009 PRESENTATIONS

51st APS DPP meeting in Dallas, TX November 2–6, 2009:

- E.M. Bass gave an invited presentation "Gyrokinetic Simulations of Enhanced Alpha Transport by Destabilized Alfven Turbulence."

- J. Candy gave an invited presentation "Predictive Gyrokinetic Transport Simulations and Application of Synthetic Diagnostics."
- M. Choi gave an invited presentation "Iterated Finite Orbit Monte Carlo Simulation with Full Wave Fields for Tokamak ICRF Wave Heating."
- A.D. Turnbull gave an invited presentation "A New View of Internal Kink Modes and their Relation to the Sawtooth Instability."

SciDAC Winter School at UC-Irvine February, 25 2009:

- R. Waltz gave a lecture "Gyrokinetic Simulations and the GYRO Code."

US-Japan RF Workshop in Toba, Japan March 16–18, 2009:

- M. Choi gave a presentation "Comparison of Monte-Carlo Ion Cyclotron Heating Model with Full-Wave Linear Absorption Model."

Scientific Grand Challenges in Fusion Energy Sciences in Washington, DC March 19, 2009:

- J. Candy gave a presentation "Status of GYRO/NEO/TGYRO."

Extreme Computing Workshop in Gaithersburg, MD March 2009:

- P.B. Snyder gave a presentation "Challenges in the Physics of the Edge Barrier Region."

Transport Modeling/Integrated Operation Scenario ITPA meeting in Naka, Japan March 31 – April 2, 2009:

- G. Staebler gave a presentation "TGLF Modeling of DIII-D ITER Scenario Discharges."

Pedestal ITPA meeting in Cadarache, France April 20–22, 2009:

- P.B. Snyder gave two presentations "Progress and Plans for the EPED1 Model and Comparison to Experiment" and "Discussion of Work Plan for ITER Urgent Issue in Pedestal Structure."

Joint EU-US Transport Task Force Workshop in San Diego, CA April 28 – May 1, 2009:

- E.M. Bass gave a presentation "Gyrokinetic Simulation of Energetic Particle Transport."
- P.B. Snyder gave a presentation "Development and Validation of a Pedestal Model for the Pedestal Height EPED1."

- J.E. Kinsey gave a presentation "Gyrokinetic Simulation Test of Quasilinear and Tracer Transport."

4th IAEA-TM Meeting on the Theory of Plasma Instabilities in Kyoto, Japan May 18–20, 2009:

- E.M. Bass gave a presentation "Gyrokinetic Simulation of Energetic Particle Transport."

1st Integrated Modeling Expert Group Annual Meeting in ITER Headquarters Cadarache, France June 23–26, 2009:

- L.L. Lao gave a presentation "Interpretive and Data Processing – IMFIT and Magnetic Reconstruction and Stability."

18th Topical Conference on RF Power in Plasma in Gent, Belgium June 24–26, 2009:

- M. Choi gave a presentation "Simulation of the DIII-D Beam Ion Heating Experiment Using a Monte-Carlo Particle Code Combined with a Full Wave Code."

2008 PRESENTATIONS

50th APS DPP meeting in Dallas, TX November 17–21, 2008:

- E.A. Belli gave an invited presentation "Drift-Kinetic Simulations of Neoclassical Transport."
- P.B. Snyder gave an invited presentation "Development and Validation of a Predictive Model for the Pedestal Height."

22nd IAEA Fusion Energy Conference in Geneva, Switzerland October 13–18, 2008:

- C. Holland gave an oral presentation "Validation of Gyrokinetic Transport Simulations Using DIII-D Core Turbulence Measurements."
- V.A. Izzo gave a presentation "RMP Enhancement Transport and Rotation Screening in DIII-D Simulations."
- P.B. Snyder gave a presentation "Pedestal Stability Comparison and ITER Pedestal Prediction."
- G.M. Staebler gave a presentation "Testing the Trapped Gyro-Landau Fluid Transport Model with Data from Tokamaks and Spherical Tori."

International Sherwood Fusion Theory Conference in Annapolis, MD April 23–25, 2008:

- E.A. Belli gave an invited presentation "Drift-Kinetic Simulations of Neoclassical transport."
- M.S. Chu gave an invited presentation "Modeling of Resistive Wall Mode with Full Kinetic Damping."

Plasma Jet Workshop at LANL January 24–25, 2008:

- P. Parks gave an invited presentation "On the Efficacy of Imploding Plasma Liners for Magnetized Fusion Target Compression."

US-Japan RF Workshop at PPPL February 27–28, 2008:

- M. Choi gave a presentation "The Coupling of 5D Particle Code with 2D Full-Wave Code for Plasma-Wave Interaction Simulation."

21st US Transport Task Force Workshop in Boulder, CO March 25–28 2008:

- J. Candy gave a presentation "Progress on TGYRO: The Steady-State Gyrokinetic Transport Code."
- M.S. Chu gave an oral presentation "Modeling of Resistive Wall Mode with Full Kinetic Damping."
- J.E. Kinsey gave an invited presentation "Development and Validation of the Next Generation Trapped Gyro-Landau-Fluid Transport Model."

Pedestal ITPA meeting in San Diego on April 30, 2008:

- P.B. Snyder gave a presentation "Developing and Testing a Predictive Model of the Pedestal Height (EPED1)."

4TH US-PRC Magnetic Fusion Collaboration Workshop in Austin, Texas May 5–6, 2008:

- V.S. Chan gave a presentation "Overview of the DIII-D Five-Year Research Plan."
- L.L. Lao gave a presentation "Development of an Integrated Modeling Tool to Support DIII-D and EAST Research and Operation."
- G. Li gave a presentation "Integration of Equilibrium, MHD Stability, and Transport to Model DIII-D Pedestal Physics and ELMs."
- Q. Ren gave a presentation "Modeling of Momentum Transport in DIII-D Discharges with and without MHD Activities."

35th European Physical Society Conference on Plasma Physics in Hersonissos, Crete, Greece June 9-13, 2008:

- R.E. Waltz gave a oral presentation "Gyrokinetic Theory and Simulation of Angular Momentum Transport."

SciDAC 2008 Conference in Seattle, WA July 13–17, 2008:

- C. Holland gave a presentation "Validating Simulations of Core Tokamak Turbulence: Current Status and Future Directions."

SCcADS Workshop on Petascale Applications and Performance Strategies in Snowbird, UT July 14–17, 2008:

- J. Candy gave a presentation "TGYRO/TGLF/NEO."

Opening Meeting for the International and Scientific Advisory Committees (CMFT) for the Center for Magnetic Fusion Theory, Chinese Academy of Science in Hefei, China September 2–3, 2008:

- V.S. Chan gave a presentation "Modeling Ion Cyclotron Heating Using Monte-Carlo Method."
- M.S. Chu gave a presentation "Modeling of Resistive Wall Mode with Full Kinetic Damping."
- L.L. Lao gave a presentation "Development of an Integrated Modeling Tool for Tokamak Research and Operation."

12th Workshop on MHD Stability Control at Columbia University, New York, NY November 18–20, 2007:

- V.A. Izzo gave a presentation "MHD Simulations of Disruption Mitigation on Alcator C-Mod and DIII-D, and Recent Experimental Highlights."

3. ADVANCES IN MHD EQUILIBRIUM AND STABILITY RESEARCH

3.1. EQUILIBRIUM RECONSTRUCTION AND ANALYTICAL DIVERTOR EQUILIBRIUM

EFIT F90/95 Development: A unified F90/95 version of EFIT for different operating platforms has been developed and tested. All grid-size related arrays have been modified to allow dynamic memory allocation so that a single EFIT version can be used for different grid sizes. A summer intern student made a significant contribution to this effort.

High Spatial Resolution EFIT Reconstruction and Force Balance: A study to investigate the convergence property of fine spatial grid (257×257, 513×513) EFIT equilibria has been completed. The results suggest that fine spatial-grid equilibria generally better satisfy the force balance constraint described by the Grad-Shafranov equation. Analysis of the EFIT equilibrium iteration algorithm also reveals that the iteration process is related to the spatial feedback stabilization of the plasma with flux control at various locations. Thus, for a converged equilibrium axisymmetric stability is generally expected with feedback. This is demonstrated numerically using a sequence of equilibria with reducing minor radii.

Analytical Tokamak Divertor Equilibrium: An analytical description of tokamak single and double null divertor equilibrium has been constructed using the homogeneous part of the exact solution of the Grad-Shafranov equation together with a particular Solovev-like solution.

3D Perturbed MHD Equilibria: Several approaches to compute 3D perturbed MHD equilibria have been investigated. These include the analytic expansion method used by Zwingmann to study the toroidal field ripple effects on 2D axisymmetric equilibrium in TORE-SUPRA with EFIT, as well as the free-energy perturbation approach used by NMA to study RWM stability. The Zwingmann's approach is expected to be valid in the regime of high n (of the order of aspect ratio) and with weak coupling to plasma (assuming the plasma response is weaker than the vacuum field). For lower n an alternative method is needed. The free-energy perturbation approach can be applied without using the virtual casing principle by making changes to the DCON and VACUUM code.

3.2. PEDESTAL MODEL DEVELOPMENT, VALIDATION, AND ANALYSIS

EPED1.6 Pedestal Height and Width Model Development and Validation: A new version of the EPED1 model, EPED1.6, has been developed that includes a new and more comprehensive model of diamagnetic stabilization. The new model has been successfully tested on a set of C-Mod, DIII-D and JET discharges, finding good initial agreement (Fig. 1). The recently developed and successfully tested predictive model for the pedestal, EPED, combines calculated peeling-ballooning and kinetic ballooning mode constraints to provide predictions of the pedestal height and width, which are first principles in that no parameters

are fit to observations. Recent comparisons and a dedicated experiment on Alcator C-Mod revealed the importance of highly accurate treatment of diamagnetic stabilization of peeling-ballooning modes, due to the high diamagnetic frequency characteristic of C-Mod. A new, diamagnetic stabilization model was therefore developed using simulation results from the BOUT++ code, which includes non-local diamagnetic effects.

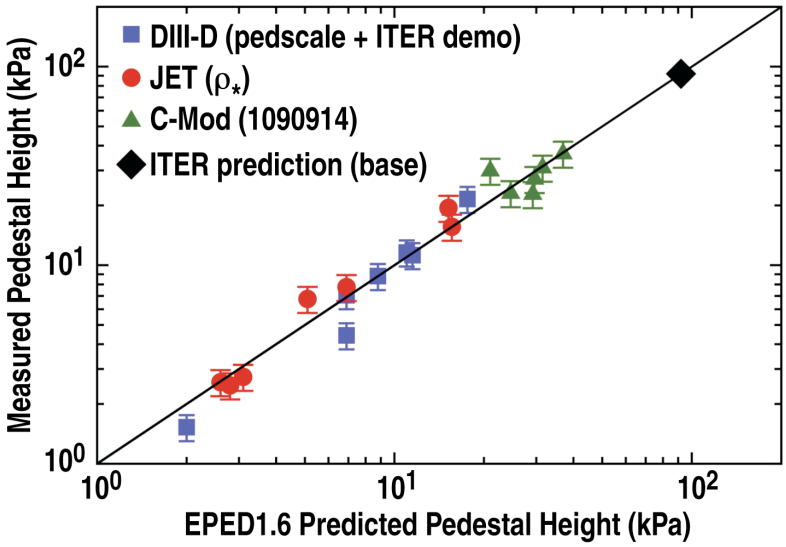

Fig. 1. The new EPED1.6 model of the pedestal height and width has been successfully tested against a data set of 21 discharges from DIII-D, JET and Alcator C-Mod, finding good agreement in predicted and observed pedestal height, across a range of more than a factor of 30. The EPED1.6 prediction for pedestal height in the ITER baseline regime is shown by a black diamond.

ITER and NSTX Pedestal Studies: The EPED1.6 pedestal model has been used to make pedestal predictions for ITER over a range of ITER operational scenarios. Pedestal height has been optimized in a study varying density and global Shafranov shift. Combining EPED pedestal predictions with TGLF core predictions to do a partial core-pedestal optimization, it is found that ITER should be able to achieve high performance operation. Results are to be presented at the 2010 IAEA fusion energy conference in Korea.

Series of NSTX discharges with varying triangularity have been studied using the ELITE code. It is found, as predicted, that reducing the triangularity on NSTX degrades ballooning stability, and causes the stability on NSTX to more closely resemble that of standard aspect ratio tokamaks, with peeling-ballooning and ballooning instabilities constraining edge profiles. As the medium to high-*n* ballooning boundary is approached in NSTX, small ELMs are observed.

The ELITE code has been used to study peeling-ballooning stability in an additional series of NSTX discharges in which the ELM frequency is reduced, and ELMs are eventually eliminated, via the application of lithium to plasma facing surfaces. It is found that the

ELMing cases operate close to the low-n kink/peeling stability boundary, and presumably ELMs are driven by these modes. As additional lithium is applied, the pedestal broadens, and eventually becomes fully stable, consistent with the disappearance of ELMs.

M3D-C1 ELM Linear Stability: Linear stability calculations with M3D-C1 have been benchmarked extensively and successfully against ELITE for intermediate toroidal mode number ($n \sim 3$–50) peeling-ballooning modes in the ideal limit. The benchmark was carried out for a variety of equilibria, including a diverted equilibrium in JT-60U geometry. The effects of including realistic resistivity and density profiles have been explored with M3D-C1. It is found that for realistic edge temperatures, a resistive model of the scrape-off layer behaves more like a force-free plasma than an ideal vacuum.

3.3. PLASMA RESPONSE TO EXTERNAL PERTURBATION FIELDS

Plasma Response Using Extended Energy Principle: By using an extended energy principle, the response of a tokamak to external magnetic perturbations has been shown to be well approximated by the vacuum response for a force free tokamak when there are no pitch resonances present. The effect of the plasma response introduces a paramagnetic effect that amplifies the vacuum response slightly. The amplification factor is inversely proportional to the aspect ratio and the safety factor. For the resonant components, paramagnetic amplification to relatively large amplitudes is possible inside of the resonant surfaces. However, the ideal MHD constraint of "frozen in flux" at the resonant surfaces imposes a diamagnetic response. The vacuum response is then a poor approximation. The effect of plasma resistivity reduces the effectiveness of the ideal MHD constraint and moves the response towards being less diamagnetic. Similar behavior is expected for a tokamak with finite β.

This extended energy principle approach provides a convenient unified framework to study tokamak plasma response including resistive and rotational effects at both the low and high frequency ranges below the Alfven frequency by minimization of free energy of the plasma together with the external coils. This minimization is achieved by directly solving the resultant Euler equations using the MARS-F code at frequencies up to the Alfven frequency (that is relevant for the TAE, BAE and RSAE modes) for different plasmas and different antenna excitation geometry. We find that plasma response with large kinetic energy has frequencies independent of the excitation geometry. The width of these response peaks can be related to the continuum damping. These frequencies can also be obtained by solving for them with small damping and with added plasma resistivity.

MARS-F Ideal and Resistive Plasma Responses: In the limit in which the plasma is assumed to behave as a vacuum, the response to external resonant perturbing non-axisymmetric magnetic fields from MARS-F has been shown to have excellent agreement with that computed previously by SURFMN, a Biot-Savart code with realistic coil arrangements. In this comparison, both SURFMN and MARS-F are also shown to agree with an analytic model for the fields produced by the external coils. With the agreement in the vacuum

response, MARS-F was then used to compute the plasma response in the ideal plasma limit. The 2D MHD response computed by MARS-F showed that the net ideal plasma plus vacuum response depends strongly on the arrangement of the external perturbing fields.

The effect of plasma resistivity on plasma response to perturbation magnetic field imposed by an external source has been studied for a rotating plasma with a separatrix. It is found that on the non-resonant helicity side, the plasma response is not much affected by plasma resistivity. On the resonant side, the overall plasma response is generally suppressed by the shielding effect caused by internal resonances. Even with resistivity and partial reconnection, the reconnection level is much lower than the full vacuum response. Thus we expect that field line stochasticity is much more reduced than that obtained with the assumption of vacuum response.

M3D-C1 Resistive Wall Boundary Conditions and Plasma Response: Resistive wall boundary conditions have been implemented into the 3D MHD code M3D-C1. The implementation of these boundary conditions utilizes the VACUUM code, which calculates the magnetic response outside the vacuum vessel given the normal field within the vessel, as calculated with M3D-C1. Stability calculations of kink modes using the resistive wall boundary conditions show good agreement with expected growth rates. This capability will allow for quantitative comparisons and modeling of RMP and RWM experimental results.

The linear plasma response to applied non-axisymmetric fields has been calculated for a series of DIII-D experiments using M3D-C1 (Fig. 2). Spitzer resistivity is used throughout the computational domain. Response calculations including two-fluid effects have also been successfully carried out. The main differences between these calculations and those done with MARS are that these are done in the time domain (as opposed to the frequency domain), and the simulation domain in M3D-C1 includes (and extends across) the separatrix in diverted configurations.

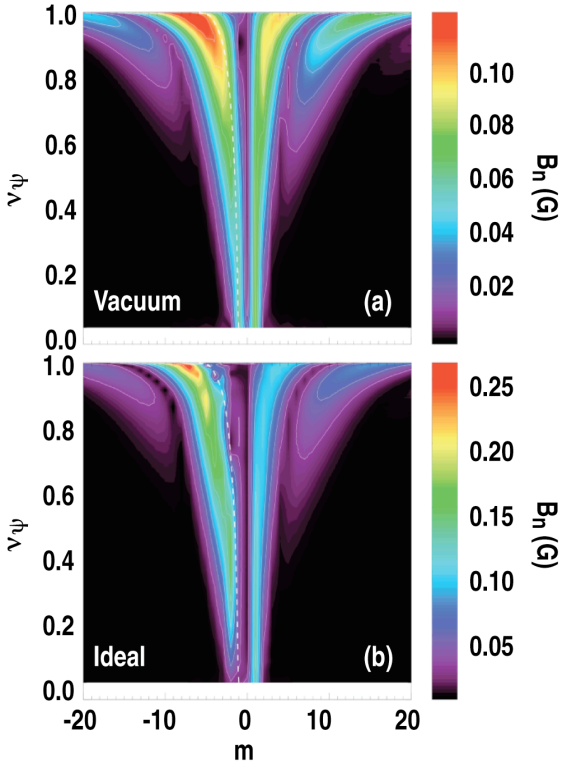

Fig. 2. Contours of the $n = 1$ normal perturbation magnetic field due to 1 kA of I-coil current without (a) and with (b) ideal plasma response as a function of poloidal mode number and square root of the normal poloidal flux for DIII-D discharge 135762 at 1815 ms.

3.4. NIMROD RMP SIMULATIONS AND DISRUPTION MODELING

NIMROD RMP Field Ramp: The implementation of time-varying externally applied error fields has been tested in NIMROD through a direct comparison between two cases run with fixed amplitude RMP fields and the identical cases with time varying boundary condition to model the I-coil current ramp beginning at $t = 0$ and achieving the same final amplitude. For these low S simulations, the RMP ramp time of 0.1 ms is comparable to a reconnection time, and the RMP fields are held fixed at their peak amplitude for several more reconnection times as a steady state solution is achieved. One pair of simulations has no plasma rotation, and thus no RMP screening, and should achieve the same steady state regardless of initial conditions.

In the fixed amplitude case, the plasma responds violently to the superimposed vacuum fields at $t = 0$, and even as a steady state is approached, a small residual $n = 1$ oscillation continues. In contrast, the identical case with the RMP field ramp obtains identical final amplitudes for the $n = 3$ and $n = 1$ field components, but does not exhibit the $n = 1$ oscillation. Two cases with toroidal plasma rotation are also compared, and also achieve very similar steady state solutions, including a large amplitude $n = 1$ oscillation associated with the plasma rotation. Although hysteresis is possible in a rotating case, it is not expected in the highly resistive and viscous regime of the simulations. In the future, hysteresis effects will be explored in a higher rotation or lower resistivity regime.

Disruption and Runaway Electron Modeling: A set of NIMROD simulations of mitigated disruptions in DIII-D, Alcator C-Mod and ITER have been completed including drift-motion calculation for a test population of runaway electrons (RE). These simulations have investigated the effects of three factors on RE confinement—plasma shape, impurity deposition profile, and device major radius. A larger RE loss fraction was found for diverted DIII-D plasmas than that limited, due to greater stochasticity in the diverted case. The loss mechanism for REs in the limited plasmas was found to be bulk $n = 1$ plasma motion into the center column, producing a signature $n = 1$ striking pattern of REs. This pattern is also observed experimentally. Using “pellet-like” versus a “gas-jet-like” Ar injection was not found to change the total loss fraction of REs in C-Mod, which was 100% in both cases. But, a change in the $n = 1$ onset time was found, which is correlated with the timing of RE losses. A comparison of simulations for all three tokamaks found that $\delta B_r/B$ near the edge varies inversely with device major radius. The result is a reduction of the RE loss fraction as device size increases.

In the DIII-D simulations, the escaping electrons striking the outer divertor early in time, and the main chamber later in time, which appears consistent with the experiments. The NIMROD radiated power spike at the time of the MHD onset has quantitative similarity to the radiated power spike in DIII-D, and the total radiated energy during the disruption shows a very close match between simulation and experiment.

With a greater number of electron orbits, the electrons can be weighted to the grid to obtain continuum quantities for visualization purposes. Contours of synchrotron radiation brightness have been produced to compare directly with DIII-D fast-camera images of runaway-electron beams (Fig. 3). A synthetic diagnostic that accounts for camera viewing angle and frequency response could be created from this data for better validation.

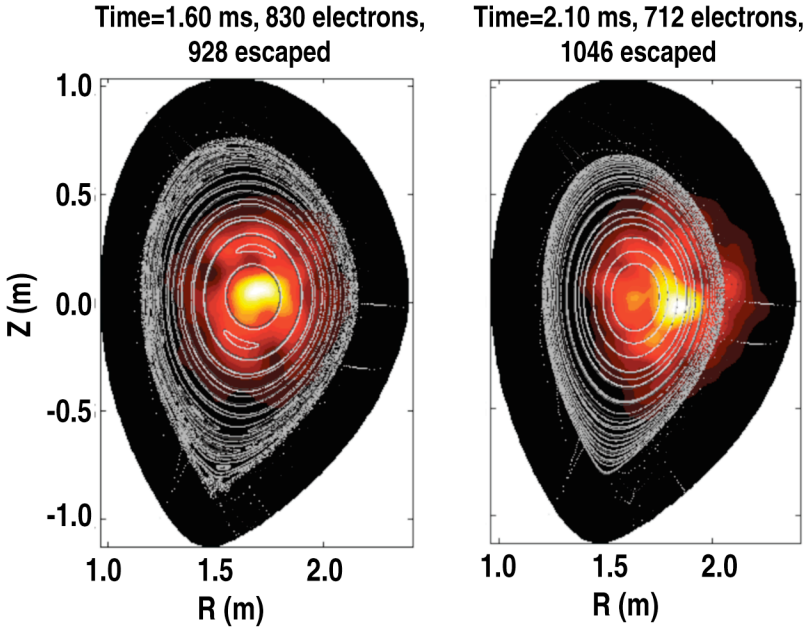

Fig. 3. Contours of synchrotron radiation brightness at 2 times in a DIII-D simulation of an Ar cooled plasma. Synchrotron light is used to determine the position of the runaway beam experimentally. In the simulation, the beam drift outward as the energy of the runaway electrons increases.

3.5. TEARING AND SAWTOOTH STABILITY MODELING

Tearing Stability Analysis: The effects of counter ECCD on tearing stability and saturated magnetic island width have been evaluated using a series of kinetic EFIT equilibria reconstructed from MSE and kinetic profile data with a local current model to represent the counter ECCD. The resistive stability properties of these equilibria are analyzed using the resistive MHD code PEST3, the NTCC island width module ISLAND, as well as the Rutherford equation. The ISLAND module evaluates saturated magnetic island widths due to NTM's based on a quasi-linear model. Initial results indicate that the tearing stability index Δ' and the saturated 3/2 island width increase strongly with a narrow ECCD width around the $q = 3/2$ surface, consistent with experimental observations (Fig. 4).

Sawtooth Stability Modeling: Calculations were performed for the DIII-D oval discharge #118164 at the sawtooth crash time with reduced β so that the mode was near marginal. The calculations showed that the eigenmode reverts to the conventional top-hat internal kink, indicating that broad counter flow of the quasi-interchange structure obtained

previously is due entirely to the finite inertia since the modes are ideally quite unstable. This sheds serious doubt on the assertion that the mode underlying the crash is quasi-interchange like and the claim that this then explains the different observed dynamics. However, a new supplementary conjecture is proposed, based on the idea that the equilibrium is being driven through the instability threshold, which reconciles the calculations and observations. In that case, the finite inertia and the corresponding broad return flow is restored at the crash time. The conjecture is consistent with the additional observation that, at least for the oval discharge, a growing helical precursor is present prior to the crash.

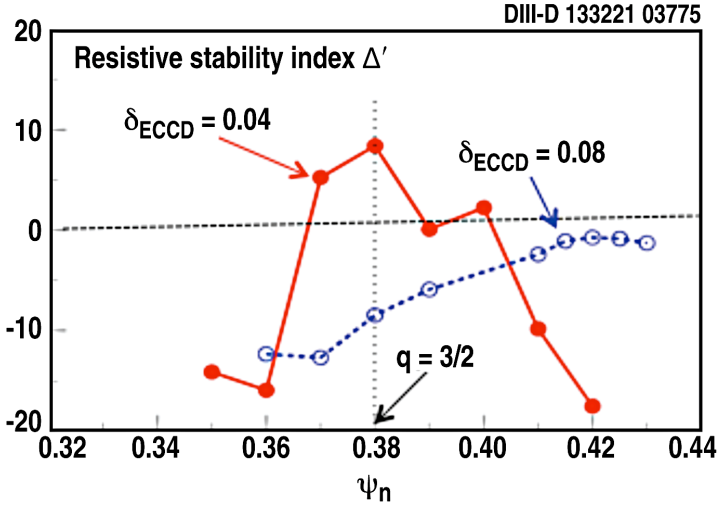

Fig. 4. Variation of the tearing stability index Δ' with normalized poloidal flux ψ_n for 2 counter ECCD widths $\delta_{ECCD} = 0.04$ (red) and 0.08 (blue).

3.6. PORTING OF NOVA-K TO GA

A new interface between EFIT and NOVA-K using the GATO mapping as a stand-alone code was completed and tested. The test used an equilibrium recalculated by the PPPL *q* solver for discharge #96043 in order to compare the result directly with that using the built-in NOVA mapping, which can only accept *q*-solver equilibria. The equilibrium was unstable to an ideal internal kink mode. All quantities required by NOVA were compared by hand and found to check out to within 5% to 10%. The final eigenvalues from NOVA using the mapped input from GATO agreed with that from the built-in NOVA mapping to within a few percent. This should greatly expand the utility of NOVA and NOVA-K since the GATO mapping can equally well accept direct equilibria from EFIT and inverse equilibria from TOQ, TEQ, and JSOLVER. In addition, the GATO mapping has the capability of mapping arbitrarily close to a diverted surface, provision for up-down asymmetry, and has considerable flexibility in options for packing the mesh at particular surfaces.

An interface was completed for transferring the radial fast ion pressure profile from ORBIT-RF to GATO and translation of this and the MHD equilibrium profiles to toroidal

flux for subsequent passing to the NOVA-K code. Coding was initiated to translate ORBIT-RF energy and pitch angle statistics into a distribution function for fitting to the NOVA-K model distribution.

3.7. GATO IMPROVEMENTS

A consistent new version of the GATO code was finalized, merging all the recent improvements, including the option to read the CORSICA i-file equilibria. The new mapping can read inverse equilibria specified on an arbitrary poloidal-angle grid and map to an arbitrary flux surface grid specified by the Jacobian. Previously the mapping input was restricted to either direct equilibria or inverse equilibria on an equal arc-length grid and the output to either equal arc-length or straight field line PEST coordinates. The complete code was also tested with the full bounds checking compiler option, which facilitated the removal of a couple of potential bugs and a number of remaining uninitiated variables. These recent changes open up the possibility of reading tokamak equilibria generated by any equilibrium code, including 2D equilibria from VMEC.

4. ADVANCES IN TRANSPORT RESEARCH

4.1. GYRO IMPROVEMENTS AND APPLICATIONS

GYRO Improvements: A new eigenvalue solver has been developed for GYRO to analyze the spectrum of unstable modes. The previous eigenvalue solver in GYRO computes the eigenvalues from the kinetic equation matrix that is large and the use of a parallel solver is required. The new eigenvalue solver drastically reduces the size by forming a matrix based on the field equations instead. Furthermore, the irrelevant velocity-space modes are eliminated. We solve the matrix problem by using the secant method. Once the converged eigenvalue is found, the eigenfunction is computed by reconstructing the field matrix with an imposed inhomogeneous constraint. Overall, the method is time efficient and has low storage requirements. This tool is presently being used to aid in studies of compressional magnetic effects in high-β NSTX plasmas, for which we find many competing modes at high $k_\theta \rho_i$.

The GYRO collision operator and transport diagnostics have been upgraded to work with compressional perturbations. Preliminary nonlinear simulations for DIII-D plasmas show that the nonlinear compressional magnetic transport is well behaved and tends to be larger than the magnetic flutter transport.

GYRO Simulation of the Subcritical β Limit: As previously reported, the 2005 β scan on Cyclone base and GA standard cases with the GYRO code was not able to operate past about half the ideal MHD critical β limit. Considerable effort has been made to operate above what appears to be a *nonlinear subcritical MHD β limit*. It was found that application of sufficient *E×B* shear could push the limit all the way to the ideal critical β with moderate transport levels. With variations of the gradients of the GA-standard case, the subcritical point drops to 35–42% of the ideal limit. By going to very large collisionality and lowering the background transport levels, we could only push up the subcritical β by a small amount. However, recently we found that lowering the gradients on the GA-standard case by 33% completely suppressed the subcritical β. Simulated β scans could operate with low-level transport up to the ideal high-*n* limit.

We conjectured that the additional pressure gradient peaks (profile corrugations) from the diamagnetic component of the zero frequency zonal flows act as an MHD unstable secondary equilibrium near half the critical β. By adding $n = 0$ pressure profile corrugations with wavelength and strength matching the nonlinear simulations to GYRO linear stability calculations, we showed that while the longest wavelength (MHD like) modes averaged over the corrugations, the growth rates of the shorter wavelength kinetic ballooning modes (KBM) has shapely increased growth rates at half the critical β. This is strong evidence for the cause of the subcritical beta.

GYRO Momentum Transport Pinch and Residual Stress: GYRO was applied to simulate several DIII-D discharges with residual stress. The shots with residual stress have very low toroidal rotation, but finite and measureable toroidal angular momentum (TAM) input from the NBI injection. The measured radial TAM transport flow represents the residual stress that presumably supports the observed spontaneous toroidal rotation (and TAM) when there is no NBI injected TAM. All the mechanisms contributing to TAM flow involve breaking the intrinsic symmetry of the toroidal gyrokinetic equation. These intrinsic symmetry-breaking mechanisms include the Kelvin-Helmholtz drive, the toroidal coriolis force, and the $E\times B$ shear. These mechanisms were illustrated in previous local flux-tube GYRO gyrokinetic simulations. Recently it was suggested that up-down asymmetry of the geometry can contribute to the residual stress. GYRO was modified to deal with up-down asymmetry and we have found this to have a negligible effect on the momentum flow. The global GYRO simulations found a surprising result: Even with small diamagnetic level $E\times B$ shear turned off, the remaining symmetry breaking from profile variation could account for all the experimental level of the core residual stress, depending on the precise ion-temperature gradient profile. However, the simulated residual stress is very sensitive to small variations of the ion-temperature gradient profile.

Residual stress refers to the remaining toroidal angular momentum (TAM) flux (divided by major radius) when the shear in the parallel velocity (and parallel velocity itself) vanishes. Previously we demonstrated with gyrokinetic (GYRO) simulations that TAM pinching from the diamagnetic level shear in the $E\times B$ velocity could provide the residual stress needed for spontaneous toroidal rotation. We have shown that the shear in the diamagnetic velocities themselves provides comparable residual stress (and level of stabilization). The sign of the residual stress, quantified by the ratio of TAM flow to ion power flow (M/P), depends on the signs of the various velocity shears (Fig. 5), as well as ion (ITG) versus electron (TEM) mode directed turbulence. The residual stress from these temperature and density gradient diamagnetic velocity shears is demonstrated in global gyrokinetic simulations of "null" rotation DIII-D discharges by matching M/P profiles within experimental uncertainty.

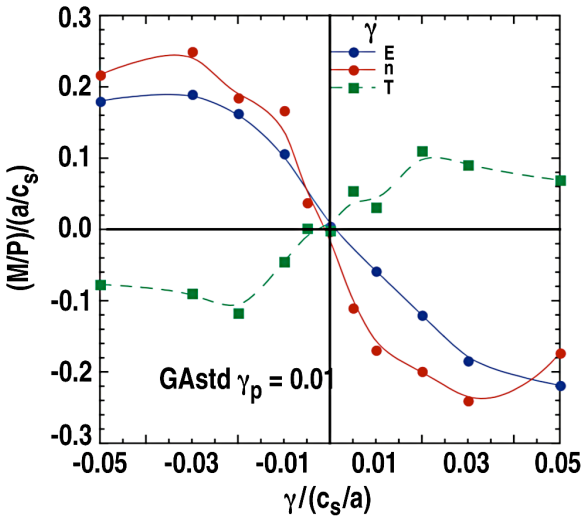

Fig. 5. Momentum-ion Power ratio (M/P) versus diamagnetic shear rates. γ_p is the parallel velocity shear, γ_E is the $E\times B$ velocity shear, and γ_n and γ_T are the density and temperature diamagnetic velocity shear.

GYRO Compressional Magnetic Perturbations: Studies of the β scaling of micro-turbulent transport were done with GYRO, which has recently been upgraded to include full electromagnetic field perturbations via the addition of the compressional

magnetic perturbations. While the effects of electromagnetic perturbations on the gyro-kinetic linear stability were found to be weak for DIII-D plasmas due to the low β, a large effect was found for NSTX plasmas.

For high-β NSTX plasmas, we find that there are no unstable modes at low $k_\theta \rho_i$ in most of the core, due to the low shear. A scan over $k_\theta \rho_i$ at $r/a = 0.7$ finds that only the low k_θ modes are unstable and even these are weakly growing. This appears to be due to the high-β gradient. In a scan over dβ/dr at low and high $k_\theta \rho_i$, we find a large effect due to the compressional magnetic effects. At low $k_\theta \rho_i$, the mode which is dominant when neglecting $\delta B_{//}$ is subdominant to another mode, which appears only when $\delta B_{//}$ is included, and it is only this mode that is unstable at the experimental value of dβ/dr. At high $k_\theta \rho_i$, we find a cascade of modes as the β gradient increases. The cascade starts at the ground state with a simple parabolic-shaped eigenmode for the electrostatic potential and increases to more complex eigenmodes with more nodes. In these simulations, very high θ resolution was needed to accurately resolve the modes due to their complex structure. With low resolution, spurious, more strongly growing computational modes often appeared.

A new compressional electron drift wave at high k_θ was identified. These modes appear only when $\delta B_{//}$ effects are included and are driven by simultaneous high β and pressure gradient. Collisional effects have been added to the new GYRO field eigenvalue solver. For simplicity, we have retained only the pitch-angle contribution to the collision operator. For our representative high-β NSTX-like plasmas, we find that collisions are stabilizing on the dominant low k_θ hybrid ITG/KBM mode. Even with large collision frequency, we surprisingly do not observe any micro-tearing instabilities (dominant or sub-dominant) for this case, most likely due to the low temperature gradient.

GYRO Gyrokinetic Pedestal Simulations: The high-*k* transport intrinsic to DIII-D plasmas as the pedestal is approached is being studied using GYRO. Initial results show that for the well-studied discharge 128913 (for which GYRO low-*k* simulations predicts significantly lower transport levels than observed experimentally), there is a significant high-*k* electron tail that markedly influences the nonlinear behavior of the simulations. The exploration of this effect is costly, however, as multi-scale simulations covering both ITG and ETG scales are required.

Steady-State Gyrokinetic Transport Development and Simulations: TGYRO development continues to move forward. Most recently we are focusing on details of the TGYRO iteration scheme. Simulations of DIII-D shot 101391 using TGYRO work very well except near the magnetic axis, for which the neoclassical transport is nearly zero, and turbulent transport vanishes. An interface to GYRO for use with both TGYRO and FMCFM has been developed.

4.2. GYRO ENERGETIC PARTICLE SIMULATIONS

GYRO Energetic-Particle Driven Turbulence: Work on the nonlinear GYRO simulations of energetic particle (EP) driven turbulence was performed under the SciDAC-GSEP funding. With sufficiently large background plasma gradients driving ITG/TEM, the additional EP transport has a "soft turn-on" beyond the linear threshold of TAE/EPM instability driven by the gradient of the EP pressure. The near threshold stiffness is only about 25% of typical ITG/TEM energy transport onset. As the EP pressure gradient is increased about 2-fold beyond the linear critical threshold gradient, the long-wavelength TAE/EPM EP transport is unbounded and runs away in time. There is only a narrow range of EP gradients where fixed gradient nonlinearly saturated states exist. The long-wavelength TAE/EPM transport is nonlinearly saturated by the zonal flows nonlinearly driven by the short-wavelength ITG/TEM turbulence. The EP transport is physically limited by the source strength, so the system does not get far beyond the critical gradient before the EP pressure gradient is quasi-linearly relaxed to the critical gradient. Remarkably the background plasma transport actually decreases at the critical gradient run-away onset due to the $E \times B$ shear generated by the run-away long-wavelength TAE/EPM modes. It seems safe to make the important conclusion that the onset of long-wavelength TAE/EPM driven EP transport does not degrade the background plasma confinement.

Dominant energetic particle modes (EPMs) and toroidal Alfvén eigenmodes (TAEs) are definitively identified in a beam-heated, shear-reversed DIII-D discharge (142111) at low values of toroidal mode number n. A third gyrokinetic species of high-energy deuterium ions (with a Maxwellian distribution) models the heating beam. Beam density is obtained from the inferred pressure profile, and effective temperature comes from a classical transport calculation. Miller-model parameters are used for the flux-surface equilibrium. The EPM shows peaks on singular (rational) surfaces as previously identified in local simulations. Observed TAEs show hybrid TAE-EPM behavior with the largest peak located between singular surfaces but tail peaks (at higher effective poloidal mode number m) on singular surfaces. A sub-dominant reverse-shear Alfvén eigenmode (RSAE), at smaller growth rate than a dominant EPM or TAE, is sometimes resolvable by analysis of initial value simulations at early times.

4.3. TGLF TRANSPORT MODEL DEVELOPMENT AND VALIDATION

TGLF Verification and Validation: New GYRO simulations including both Miller geometry and collisions have been included in the existing GYRO transport database extending the total number of simulations in the database to 191. The 191 cases were then compared against the results from TGLF-09 yielding RMS errors in (χ_i, χ_e) of [13%, 16%]. This can be compared to the results using TGLF-APS07 that has errors of [24%, 23%].

The TGYRO code has also been used as an additional tool for verifying the XPTOR/TGLF results. The goal has been to verify the TGLF ITER predictions obtained

using the XPTOR code against TGYRO predictions using local GYRO flux tube simulations to compute the turbulent energy transport. The benchmarking of TGYRO against XPTOR using TGLF-09 was carried out for a DIII-D L-mode discharge. The GYRO results are in good agreement with the TGLF-09 results.

TGLF with original collision model (APS07) was validated against a profile database of 96 L- and H-mode discharges. Recent work has focused on testing TGLF with the new collision model (APS09) against DIII-D and JET hybrid discharges. The results are shown in Fig. 6. There are 30 DIII-D and 4 JET hybrid discharges included in the database. The predicted temperature profiles agree with the experimental data.

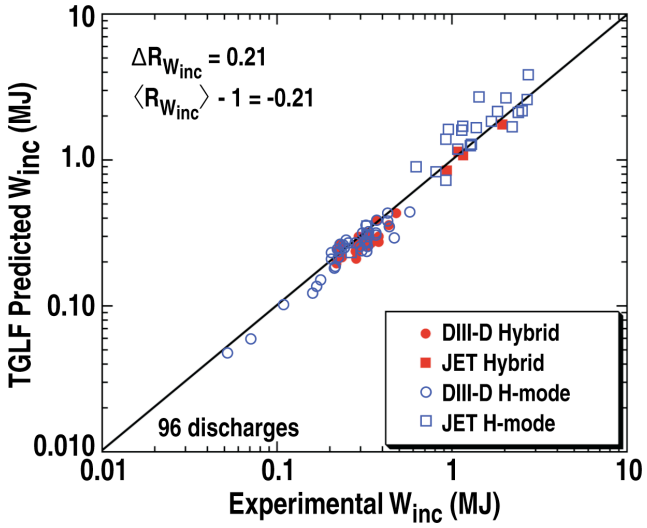

Fig. 6. Comparison of TGLF predicted incremental stored energy against experimental values for 30 DIII-D and 4 JET hybrid discharges, plus 40 DIII-D and 22 JET H-mode discharges.

TGLF Sensitivity Study: A sensitivity study of TGLF analyses of DIII-D hybrid discharges shows that the temperature offsets become increasingly negative as the boundary location is extended outward into the pedestal region, as a result of the energy transport is being over predicted. This trend appears to be opposite of what is found in the near edge region of L-mode discharges.

TGLF Finite β Transport Effects: In recent TGLF modeling studies of DIII-D ITER demonstration discharges, it was found that finite β effects are important in discharges where $\beta_N > 3$. In several hybrid and steady-state cases, a noticable reduction in the electron energy transport due to finite β was observed across the entire radius (Fig. 7). Very little change was observed in the ion channel. These results motivate future work involving the use of real EFIT equilibria instead of Miller geometry in TGLF and also GYRO EM simulations of ETG modes.

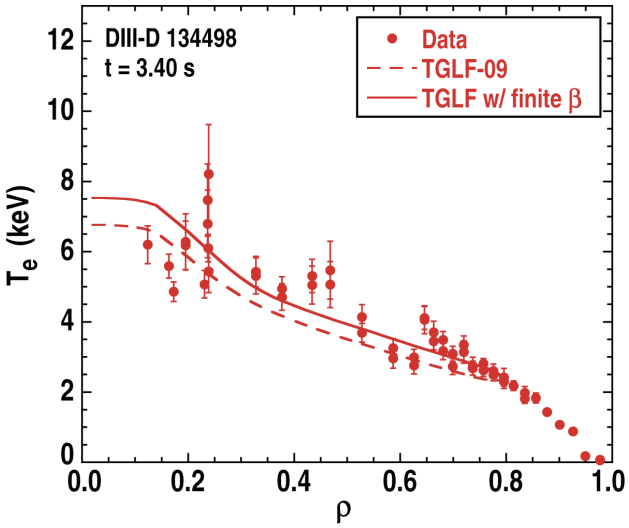

Fig. 7. TGLF predicted electron temperature profiles for a high β_N DIII-D hybrid discharge 134498 with (solid curve) and without (dashed curve) finite β effects included in the model.

TGLF Momentum Transport: More GYRO runs with parallel velocity shear were made in order to verify the TGLF momentum transport model. Problems were found with TGLF for these runs. The first problem was that the eigenmode solver was finding a narrow width mode that then gives a poor agreement with GYRO when refined with more basis functions. A method to suppress the low-width branch was found by multiplying the parallel velocity shear by the normalized mode width. This fix gives much better agreement for the linear growth rates, energy and particle fluxes with GYRO. However, a second problem still exists. The momentum flux computed with TGLF agrees with GYRO for low parallel velocity shear (where the mode is ITG), but drops a factor of 2 below the GYRO result once the Kelvin-Helmholtz (KH) mode becomes dominant. This may be a breakdown of the quasi-linear theory or just an inaccurate quasi-linear weight from TGLF for the KH mode. Limited comparison with data indicates that the larger GYRO momentum flux is closer to experiment. Unless some other solution is found, TGLF will just multiply the momentum flux quasi-linear weight by 1.9 to agree with GYRO at the higher parallel velocity shears. More GYRO runs are needed in order to finalize the model.

The two fitting coefficients for the new generalized quench rule were finalized using new GYRO runs. A careful tracking of the dependence on the signs of the toroidal and poloidal magnetic fields uncovered an interesting sign flip for the $E\times B$ shear induced momentum flux. This is being checked with a GYRO run using the new version of GYRO with the field signs included. The result confirms the sign dependence published by Peeters for his GKW code. It needs to be checked by GYRO because TGLF has no way to determine the sign of the radial mode number linearly.

TGLF Pedestal Modeling: A few attempts at applying TGLF within the H-mode pedestal region have also been performed. Using a high resolution transport analysis of DIII-D H-mode #98889, TGLF was successful in predicting the energy transport with the boundary conditions extended out to a radius of $\rho = 0.99$. While the predicted T_e profile is somewhat too high near the top of the pedestal, the model was successful in predicting the formation of an H-mode pedestal. Analysis of the diffusivities show that the ion channel is mildly turbulent and the ETG modes contribute to roughly half of the electron energy transport.

TGLF Fusion Projection for ITER: Using the TGLF APS09 model, numerous ITER fusion projections have been performed examining the impact of the new collision model, shaped geometry, density peaking, and finite β. For flat density profiles the results obtained for TGLF using shifted circle geometry are nearly identical to those obtained using the GLF23 model. The predictions using TGLF with the original collision model (APS-07) are pessimistic compared to the GLF23 results. Using the new collision model the fluxes are reduced and the fusion projections are more optimistic and closer to those found using GLF23.

TGLF Release: The TGLF linear stability and quasi-linear transport code is available for public distribution. The package includes a stand-alone driver for computing linear drift wave eigenmodes or quasi-linear fluxes. The TGLF model has been extensively verified against fully gyrokinetic linear stability calculations and non-linear turbulence simulations using the GYRO code. The TGLF model has proven to be a more accurate model of the gyrokinetic results than its widely used predecessor GLF23. As reported at the 2007 APS conference, the TGLF model predicts the core temperature profiles for a database of more than 100 discharges from three tokamaks with greater accuracy than GLF23. After filling in a user agreement form, a copy of the TGLF source code can be downloaded from its webpage.

4.4. NEOCLASSICAL TRANSPORT AND FLOW

NEO Deuterium Edge Flows and Poloidal Rotation Studies: NEO has been used to analyze the deuterium ion flow of DIII-D L-mode plasmas in the edge. For these studies, a new method has been developed to determine the shift in the parallel flow due to the radial electric field based on using the carbon toroidal flow measurements in the core as a calibration. The NEO results for the deuterium flow, which were done inside the separatrix, and the measurements, which were done outside the separatrix, qualitatively approach each other as ρ approaches 1, indicating that the flow remains essentially neoclassically driven even close to the plasma edge. Interestingly, we also find that the deuterium flows are close to the impurity carbon toroidal flow measurements in the core, but the two flows become uncorrelated in the steep edge gradient region, with the deuterium flow becoming much larger than the carbon flow.

NEO has also been used to analyze the carbon impurity poloidal flow in NSTX to aid in the planning of the joint NSTX/DIII-D poloidal rotation experiment. For both low and high-field shots, we find that NEO agrees better with the experimental measurements than both NCLASS and GTC-NEO. The improvement with NEO agrees with benchmarks that we have previously done in simple limits and is due to improvements in the treatment of the local physics by using a direct kinetic approach. While finite-orbit-width effects, which are included in GTC-NEO but not in NCLASS, are believed to be larger in NSTX than in DIII-D due to the low field and small aspect ratio, studies of the non-local corrections with NEO find these effects to be only a few percent. For the planned DIII-D experiments, which are designed to match the NSTX discharges, preliminary NEO calculations for the same parameters as the high-field NSTX case but with large aspect ratio predict a significantly enhanced effect on the impurity poloidal rotation.

Finite-Orbit-Width/Orbit-Squeezing Effects on Neoclassical Transport: The effects of orbit squeezing on the ion neoclassical transport in tokamak plasmas have been studied analytically and numerically via solution of the hierarchy of drift-kinetic equations ordered in ρ_i^*. For the simple case of a single ion species with uniform temperature and assuming s-α geometry, an analytic solution has been derived for the first-order (standard local neoclassical) and second-order distribution functions in both the banana and Pfirsch-Schluter collisional regimes and for the third-order distribution function in the latter regime. The third-order solution is necessary to study the non-local transport corrections due to finite-orbit-width effects, since the transport coefficients from the second-order solution are zero for up-down symmetric plasmas. We find that the radial dependence of the non-local transport has a coupled dependence on higher-order derivatives of the geometry parameters, the density gradient, and the radial electric field. This dependence is significantly more complicated than the usual orbit-squeezing factor would imply. Furthermore, we find that inclusion of the nonlinear collision operator is crucial. Specifically, the solubility condition essentially removes the θ-average of the collisionless part of the solution, thus reducing its contribution to $O(r/R)$. The largest component to the higher-order solution then instead results from the nonlinear collision dynamics.

NC Neoclassical Transport: The Kovrizhnikh collision operator has been implemented in the neoclassical transport MATLAB code NC for neoclassical ion transport. Using this operator, the code was successfully benchmarked against existing numerical results from NEO and the work of Bolton and Ware. In extreme parameter ranges for the inverse aspect ratio (around 0.025) and collisionality $\nu_* \sim 0.003$, the code result agrees with the analytic thermal conductivity in the banana regime with about 5% accuracy. Other enhancements include calculations of the full distribution function and the poloidal electric field.

5. ADVANCES IN RF HEATING AND FUELING RESEARCH

5.1. ORBIT-RF SIMULATIONS OF ICRF HEATING SCENARIOS

Iterative simulations of 5D finite-orbit Monte-Carlo code ORBIT-RF coupled with 2D full-wave code All-ORders Spectral Algorithm AORSA including quasi-linear and collisional orbit diffusion reproduce reasonably experimental observations in enhanced neutron reaction, spectra and outward spatial shifts of measured FIDA signals from the magnetic axis in DIII-D and NSTX moderate to high harmonic ICRF heating experiments. The outward radial shift is due to large orbit drifts of fast ions across the magnetic surfaces, which cannot be reproduced when finite drift orbit effect is ignored (Fig. 8). Preliminary ORBIT-RF/AORSA simulations for proposed fundamental minority ICRF heating scenarios in ITER and KSTAR suggest that finite orbit effect may significantly modify fast ion distribution in velocity space, depending on applied ICRF power density. At higher ICRF power density scenario in KSTAR (0.38 MW/m^3), finite orbit effect modifies symmetrically distorted distribution to asymmetric rabbit ear feature, whereas at lower power density scenario in ITER (0.026 MW/m^3) it appears to average out strong anisotropic distribution to more isotropic distribution.

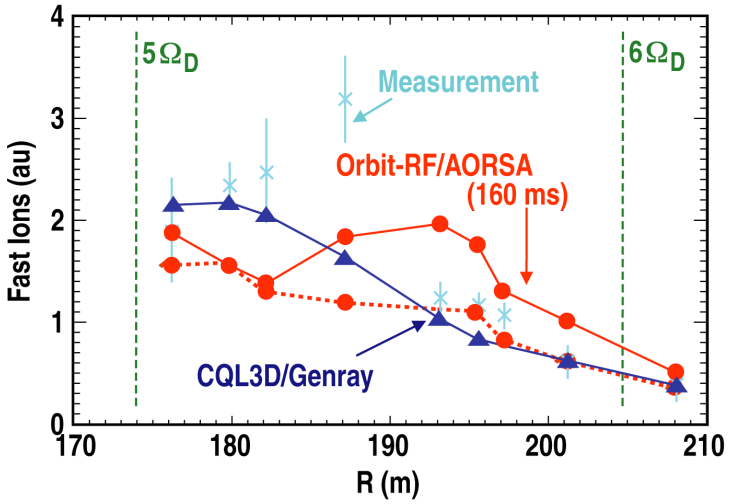

Fig. 8. Comparison of fast-ion spatial profiles from ORBIT-RF/AORSA (dashed curve for 80 ms simulation and solid curve for 160 ms simulation) against CQL3D/GENRAY and FIDA measurements for a DIII-D 5th harmonic ICRF heating discharge 122993.

5.2. MPI DISRUPTION AND RUNAWAY ELECTRON MITIGATION STUDY

A first time-dependent analytical model for the volumetric heating and expansion of small room-temperature solid pellets interacting with multi-MeV runaway electrons (RE) was constructed. The model, which recognizes the importance of the super-critical pressure-volume response of the pellet to intense heating, is relevant to heating and vaporization of

small pellets under conditions where the pellet size is small relative to the RE stopping distance (range) and where the pellet mass is small enough not to perturb the local RE current density and energy content of the RE channel. For avalanche runaways where the average energy is ~ 20 MeV, The model provides insights both for interpreting the present experimental results and for how pellet size, material and injection velocity can be optimized in future experiments to facilitate using of small "non-perturbative" diagnostic pellets to provide data on the magnitude and profile of runaway current density and energy content deep within high-current RE discharges.

An analytical model was also developed to determine whether "mature" high-current RE once formed, could be stopped after a massive gas injection. The important model assumption is that mature runaways have the energy distribution function that is expected if the avalanche production mechanism were responsible for their formation. A remarkable property was found, that was not obvious or known in the literature, namely, the *decay rate* of the RE current when $E < E_{crit}$ is equal and opposite to the (avalanche) growth rate when $E > E_{crit}$. We took advantage of this symmetry property to develop a modified Grad-Shafranov Equation (GSE) for the mature runaway channel in order to discover how we could destroy the RE beam over its long lifetime (~ 50 to 100 ms in DIII-D), i.e., before the RE current channel contacts the wall by the VDE. We obtained a numerical solution of the GSE in the cylindrical limit. The RE current-profile tends to be much more centrally peaked relative to the initial plasma current profile, yet $q_0 > 1$ so that the RE current channel is always stable to internal kinks, in qualitative agreement with experiments on DIII-D. It was found that the current profile displays an interesting profile consistency or "resilience", as it is practically independent of the profile of the initial RE seed component preformed in the thermal quench phase. The numerical solution is also weakly non-stationary with a secular time dependence that can be traced to the slow dissipation, or "erosion", of the RE plateau and associated inductive energy due to collisions on the cold background electrons. The model predicts massive RE currents could be completely eroded in ITER in a span of only 200 ms by a combination of a modest particle densification, of the order of twenty times, and negative surface loop voltage application with $E_{sur} \sim 1$ V/m. The model is being used to interpret recent DIII-D experiments where this effect was first discovered

6. ADVANCES IN INTEGRATED MODELING

6.1. IMFIT DEVELOPMENT AND APPLICATIONS

A first version of the IMFIT Integrated Modeling and Fitting tool has been released for public use. IMFIT provides a convenient central platform to perform equilibrium, transport, and stability analysis using tools such as EFIT, ONETWO, GATO, ELITE, DCON, and PEST3. IMFIT also provide convenient GUI's to support experimental data viewing and analysis using tools such as EFITViewer, REVIEW+, GAProfiles, and PLOT12. A GUI to perform kinetic EFIT analysis is also available, as well as support for other tokamak devices such as EAST, ITER, and SST-1. New ones can be conveniently added. More information can be found at the IMFIT web site, as well as through various "Help" buttons available within IMFIT.

6.2. ONETWO TRANSPORT CODE DEVELOPMENT

TGLF Implementation and Testing: A version of the TGLF confinement model was installed and operational in the ONETWO transport code based on the GCNMP global Newton solver. To deal with extremely computationally intensive models such as TGLF, several improvements to GCNMP were made. These include a Jacobian-free solution method, finite-difference form of the transport equations in terms of fluxes rather than diffusivities, and a "compact derivative" scheme that uses all grid points to define higher-order derivatives across the entire computational grid simultaneously. Compact derivatives provide a smoother representation of derivatives compared to the standard finite representation method.

Benchmarking calculations against the XPTOR transport code were carried out for two DIII-D discharges and a FDF configuration. ONETWO/GCNMP results with TGLF agree with those from XPTOR and the experimentally measured profiles to within 10–15% difference. The predicted temperature profiles from GCNMP are smoother when the compact- derivative approach is used in the analysis.

Version 5.3 of the ONETWO transport code was completed. This new ONETWO version writes a state file that can be used to drive the parallel transport code GCNMP. GCNMP in turn produces a similar state file at selected times. Any of the state files can be used to restart computations either in ONETWO or GCNMP.

7. PUBLICATIONS

PRIMARY THEORY AUTHORS FOR 2010

E. Bass and R.E. Waltz, "Gyrokinetic simulation of mesoscale energetic particle-driven Alfvénic turbulent transport embedded in microturbulence," accepted for publication in Phys. Plasmas.

E. Belli and J. Candy, "Fully Electromagnetic Gyrokinetic Eigenmode Analysis of High-Beta Shaped Plasmas" accepted for publication in Phys. Plasmas.

M.S. Chu and M. Okabayashi, "Stabilization of the External Kink and Resistive Wall Mode," accepted for publication in Plasmas Phys. Control. Fusion.

M. Choi, D. Green, W.W. Heidbrink, R.W. Harvey, D. Liu, V.S. Chan, L.A. Berry, E.F. Jaeger, L.L. Lao, R.I. Pinsker, M. Podesta, D.N. Smithe, J.M. Park, and P. Bonoli, RF SciDAC, and SWIM Team, "Iterated Finite-Orbit Monte Carlo Simulations with Full-Wave Fields for Modeling Tokamak," Phys. Plasmas **17**, 056102 (2010).

N.M. Ferraro, S.C. Jardin, and X. Luo, "Boundary Conditions with Reduced Quintic Finite Elements," submitted to J. Comp. Phys.

N.M. Ferraro, S.C. Jardin, and P.B. Snyder, "Ideal and Resistive Edge Stability Calculations with M3D-C1," accepted for publication in Phys. Plasmas.

W. Guttenfelder and J. Candy, "Resolving electron scale turbulence in spherical tokamaks with flow shear," submitted to Phys. Plasmas.

J.E. Kinsey, G.M. Staebler, and C.C. Petty "TGLF Transport Modeling of DIII-D Hybrid Discharges," submitted to Phys. Plasmas.

Q. Ren, M.S. Chu, and L.L. Lao, "High Spatial-Resolution Equilibrium Reconstruction and its Force Balance Analysis," to be submitted to Plasmas Phys. Control. Fusion.

R. Samulyak, P.B. Parks, and L. Wu, "Spherically Symmetric Simulation of Plasma Liner Driven Magnetoinertial Fusion," Phys. Plasmas **17**, 092702 (2010).

R. Srinivasan, L.L. Lao, and M.S. Chu, "Analytical Description of Tokamak Equilibrium with Divertor Configuration," Plasmas Phys. Control. Fusion, **52**, 035007 (2010).

G.M. Staebler and J.E. Kinsey, "Electron Collisions in the trapped gyro-Landau fluid transport mode," accepted for publication in Phys. Plasmas.

R.E. Waltz, "Nonlinear Subcritical Magnetohydrodynamic Beta Limit," Phys. Plasmas **17**, 072501 (2010).

PRIMARY THEORY AUTHORS FOR 2009

C. Angioni, J. Candy, E. Fable, M. Maslov, A.G. Peeters, R.E. Waltz, and H. Weisen, "Particle Pinch and Collisionality in Gyrokinetic Simulations of Tokamak Plasma Turbulence," Phys. Plasmas **16**, 060702 (2009).

E.A. Belli and J. Candy, "An Eulerian Method for Solution of the Multispecies Drift-Kinetic Equation," Plasmas Phys. Control. Fusion **51**, 075018 (2009).

S. Braun, P. Helander, E.A. Belli, and J. Candy, "Effects of Impurities on Collisional Zonal-Flow Damping in Tokamaks," Plasmas Phys. Control. Fusion **51**, 065011 (2009).

J. Breslau, N.M. Ferraro and S.C. Jardin, "Some Properties of the M3D-C1 Form of the 3D Magnetohydrodynamics Equations," Phys. Plasmas **16**, 092503 (2009).

J. Candy, C. Holland, R.E. Waltz, M.R. Fahey, and E. Belli, "Tokamak Profile Prediction Using Direct Gyrokinetic and Neoclassical Simulation," Phys. Plasmas **16**, 060704 (2009).

J. Candy, "A Unified Method for Operator Evaluation in Local Grad-Shafranov Plasma Equilibria," Plasmas Phys. Control. Fusion **51**, 105009 (2009).

A. Castali, T. Gerbaud, P. Hennequin, C. Bourdelle, J. Candy, F. Clariet, X. Garbet, V. Grandgirard, O.D. Gurcan, S. Heuraux, G.T. Hoang, C. Honore, F. Imbeaux, R. Sabot, Y. Sarazin, L. Vermare, and R.E. Waltz, "Turbulence in the TORE SUPRA Tokamak: Measurements and Validation of Non-linear Simulations," Phys. Rev. Lett. **102**, 165005 (2009).

A. Casati, T C. Bourdelle, X. Garbet, F. Imbeaux, J. Candy, F. Clairet, G. Dif-Pradalier, G. Falchetto, T. Gerbaud, V. Grandgirard, O.D. Gurcan, P. Hennequin, J. Kinsey, M. Ottaviani, R. Sabot, Y. Sarazin, L. Vermare, and R.E. Waltz, "Validating a Quasi-Linear Transport Model versus Nonlinear Simulations," Nucl. Fusion **49**, 085012 (2009).

M. Choi, V.S. Chan, L.A. Berry, E.F. Jaeger, D. Green, P. Bonoli, J. Wright, and RF SciDAC Team, "Comparison of Monte-Carlo Ion Cyclotron Heating Model with Full-Wave Linear Absorption Model," Phys. Plasmas **16**, 052513 (2009).

N.M. Ferraro and S.C. Jardin, "Calculations of Two-Fluid Magnetohydrodynamic Axisymmetric Steady-States," J. Comp. Phys. **228**, 7742 (2009).

J.R. Gary, J. Candy, J. Cobb, R.H. Cohen, T. Epperly, D.J. Estep, S. Krasheninnikov, A.D. Malony, D.C. McCune, L. McInnes, A. Pankin, S. Balay, J.A. Carlsson, M.R. Fahey, R.J. Groebner, A.H. Hakim, S.E. Kruger, M. Miah, A. Pletzer, S. Shasharina, S. Vadlamani, D. Wade-Stein, T.D. Rognlien, A. Morris, S. Shende, G.W. Hammett, S. Indireshkumar, A. Yu Pigarov, and H. Zhang, "Concurrent, Parallel, Multiphysics Coupling in the FACETS Project," J. Phys.: Conf. Ser. **180**, 012056 (2009).

J.D. Hanson, S.P. Hirshman, S.F. Knowlton, L.L. Lao, E.A. Lazarus, and J.M. Shields, "V3FIT: a Code for Three-Dimensional Equilibrium Reconstruction," Nucl. Fusion **49**, 075031 (2009).

C. Holland, A.E. White, G.R. McKee, M.W. Schafer, J. Candy, R.E. Waltz, L. Schmitz, and G.R. Tynan, "Implementation and Application of Two Synthetic Diagnostics for Validating Simulations of Core Tokamak Turbulence," Phys. Plasmas **16**, 052301 (2009).

V.A. Izzo, P.B. Parks, and L.L. Lao, "DIII-D and ITER Rapid Shutdown with Radially Uniform Deuterium Delivery," Plasmas Phys. Control. Fusion **51**, 105004 (2009).

L. Lin, M. Porkolab, E.M. Edlund, M. Greenwald, N. Tsujii, J. Candy, R.E. Waltz, and D.R. Mikkelsen, "Studies of Turbulence and Transport in Alcator C-Mod Ohmic Plasmas with Phase Contrast Imaging and Comparison with gyro-kinetic Simulations," Plasmas Phys. Control. Fusion **51**, 065006 (2009).

P.B. Parks, T. Lu, and R. Samulyak, "Charging and E×B Rotation of Ablation Clouds Surrounding Refueling Pellets in Hot Fusion Plasmas," Phys. Plasmas **16**, 060705 (2009).

C. I. Pusztai, T. Fulop, J. Candy, and R.J. Hastie, "Collisional Model of Quasilinear Transport Driven by Toroidal Electrostatic Ion Temperature Gradient Modes," Phys. Plasmas **16**, 072305 (2009).

J.P. Qian, L.L. Lao, Q.L. Ren, H. Rinderknecht, F. Volpe, C. Zhang, and B.N. Wan. "Equilibrium Reconstruction of Plasma Profiles Based on Soft X-Ray Imaging in DIII-D," Nucl. Fusion **49**, 025003 (2009).

J. Qian, B. Wan, L.L. Lao , S. Biao, S.A. Sabbagh, Y. Sun, D. Liu, B. Xiao, Q. Ren, X. Gong, and J. Li, "Equilibrium Reconstruction in EAST Tokamak," Plasma Sci. Technol. **11**, 142 (2009).

J. Qian, B. Wan, S. Biao, L.L. Lao, B. Xiao, J. Li, S. Lin, and Z. Luo, "Observational of Poloidal Current Flowed to the Vessel after Failure of Vertical Position feedback Control in EAST Tokamak," Chinese Phys. B **18**, 1172 (2009).

Q. Ren, M.S. Chu, L.L. Lao, H. St. John, R. La Haye, Y.M. Jeon, Z. Cheng, D. Zhou, G. Li, J.M. Park, and J. deGrassie, "Momentum Transport in DIII-D Discharges with and without Magnetohydrodynamic (MHD) Activity," Plasma Sci. Technol. **11**, 127 (2009).

Y. Shen, J. Dong, H. He, and A.D. Turnbull, "Preliminary Study of Ideal Operational MHD Beta Limit in HL-2A Tokamak Plasmas," Plasma Sci. Technol. **11**, 131 (2009).

P.B. Snyder, R.J. Groebner, A.W. Leonard, T.H. Osborne, and H.R. Wilson, "Development and Validation of a Predictive Model for the Pedestal Height," Phys. Plasmas **16**, 056118 (2009).

P.B. Snyder, N. Aiba, M. Beurskens, R.J. Groebner, L.D. Horton, A.E. Hubbard, J.W. Hughes, G.T.A. Huysmans, Y. Kamada, A. Kirk, C. Konz, A.W. Leonard, J. Lönnroth, C.F. Maggi, R. Maingi, T.H. Osborne, N. Oyama, A. Pankin, S. Saarelma, G. Saibene, J.L. Terry, H. Urano, and H.R. Wilson "Pedestal Stability Comparison and ITER Pedestal Prediction," Nucl. Fusion **49**, 085035 (2009).

R.E. Waltz, A. Casati, and G. Staebler, "Gyrokinetic Simulation Test of Quasilinear and Tracer Transport," Phys. Plasmas **16**, 072303 (2009).

S.K. Wong and V.S. Chan, "Self-Consistent Electric Field and Neoclassical Angular Momentum Flux," Phys. Plasmas **16**, 122507 (2009).

PRIMARY THEORY AUTHORS FOR 2008

E.A. Belli and J. Candy, "Kinetic Calculation of Neoclassical Transport including Self-Consistent Electron and Impurity Dynamics," Plasmas Phys. Control. Fusion **50**, 095010 (2008).

Y.Q. Liu, M.S. Chu, C.G. Gimblett, and R.J. Hastie "Magnetic Drift Kinetic Damping of the Resistive Wall Mode in Large Aspect Ratio Tokamaks," Phys. Plasmas **15**, 092505 (2008).

V.A. Izzo, D.G. Whyte, R.S. Granetz, P.B. Parks, E.M. Hollmann, L.L. Lao, J.C. Wesley, "MHD Simulations of Massive Gas Injection into Alcator C-Mod and DIII-D Plasmas," Phys. Plasmas **15**, 056109 (2008).

V.A. Izzo and I. Joseph, "RMP Enhanced Transport and Rotational Screening in Simulations of DIII-D Plasmas," Phys. Plasmas **48**, 115004 (2008).

J.E. Kinsey, G.M. Staebler, and R.E. Waltz, J. Candy, "The First Transport Code Simulations Using the TGLF Model," Phys. Plasmas **15**, 055908 (2008).

G. Li, S.J. Wang, L.L. Lao, A.D. Turnbull, M.S. Chu, D.P. Brennan, R.J. Groebner, and L. Zhao, "Ideal MHD Stability of Double Transport Barrier Plasmas in DIII-D," Nucl. Fusion **48**, 015001 (2008).

P. Parks, "On the Efficacy of Imploding Plasma Liners for Magnetized Fusion Target Compression," Phys. Plasmas **15**, 062506 (2008).

R.E. Waltz and C. Holland, "Numerical Experiments on the Drift Wave – Zonal Flow Paradigm for Nonlinear Saturation," Phys. Plasmas **15**, 122503 (2008).

R.E. Waltz and G.M. Staebler, "Gyrokinetic Theory and Simulation of Turbulent Energy Exchange," Phys. Plasmas **15**, 014505 (2008).

S.K. Wong, V.S. Chan, and W.M. Solomon, "Poloidal Velocity of Impurity Ions in Neoclassical Theory," Phys. Plasmas **15**, 082503 (2008).

ACKNOWLEDGMENT

This work supported by the U.S. Department of Energy under Grant No. DE-FG02-95ER54309.